Thermally stabilized PCF-based sensor for temperature measurements up to 1000°C

Gianluca Coviello[1], Vittoria Finazzi[1*], Joel Villatoro[1], and Valerio Pruneri[1,2]

[1]*ICFO - Institut de Ciencies Fotoniques, Mediterranean Technology Park, 08860 Castelldefels (Barcelona), Spain*

[2]*ICREA - Institució Catalana de Recerca i Estudis Avanats, 08010, Barcelona, Spain*

vittoria.finazzi@icfo.es

Abstract: We report on the development of a stable Photonic Crystal Fiber (PCF) based two-mode interferometric sensor for ultra-high temperature measurements (up to 1000°C). The device consists of a stub of PCF spliced to standard optical fiber. In the splice regions, the voids of the PCF are fully collapsed, thus allowing the excitation and recombination of two core modes. The device spectrum exhibits sinusoidal interference pattern which shifts with temperature. We show that, despite being compact and robust, the proposed sensor head needs a quite long burn in (thermal annealing) to achieve an adequate and stable functionality level. The burn in process eliminates the residual stress in the fiber structure, which had been accumulated during the drawing phase, and changes the glass fictive temperature.

OCIS codes: (060.4005) Microstructured fibers; (060.5295) Photonic crystal fibers; (060.2370) Fiber optics sensors; (120.3180) Interferometry; (280.4788) Optical sensing and sensors; (280.6780) Temperature; (160.0160) Materials.

References and links

1. A. Rose, "Devitrification in annealed optical fiber," J. Lightwave Technology, **15**(5), 808–814 (1997).
2. A. H. Rose and T. J. Bruno, "The observation of OH in annealed optical fiber," J. Non-Cryst. Solids **231**(3), 280 – 285 (1998).
3. S. Trpkovski, D. J. Kitcher, G. W. Baxter, S. F. Collins, and S. A. Wade, "High-temperature-resistant chemical composition Bragg gratings in Er3+-doped optical fiber," Opt. Lett. **30**, 607–609 (2005).
4. S. Bandyopadhyay, J. Canning, M. Stevenson, and K. Cook, "Ultrahigh-temperature regenerated gratings in boron-codoped germanosilicate optical fiber using 193 nm," Opt. Lett. **33**, 1917–1919 (2008).
5. K. Cook, A. A. P. Pohl, and J. Canning, "High-temperature type IIa gratings in 12-ring photonic crystal fibre with germanosilicate core," J. Europ. Opt. Soc. Rap. Public. **3**, 08,031 (2008).
6. V. I. Kopp, V. M. Churikov, G. Zhang, J. Singer, C. W. Draper, N. Chao, D. Neugroschl, and A. Z. Genack, "Single- and double-helix chiral fiber sensors," J. Opt. Soc. Am. B **24**(10), A48–A52 (2007).
7. H. Y. Choi, K. S. Park, S. J. Park, U. C. Paek, B. H. Lee, and E. S. Choi, "Miniature fiber-optic high temperature sensor based on a hybrid structured FabryPerot interferometer," Opt. Lett. **33**, 2455–2457 (2008).
8. M. Fokine, "Formation of thermally stable chemical composition gratings in optical fibers," J. Opt. Soc. Am. B **19**(8), 1759–1765 (2002).
9. A. Kersey, M. Davis, H. Patrick, M. LeBlanc, K. Koo, C. Askins, M. Putnam, and E. Friebele, "Fiber grating sensors," J. Lightwave Technol. **15**(8), 1442–1463 (1997).
10. D. Monzon-Hernandez, V. P. Minkovich, and J. Villatoro, "High-temperature sensing with tapers made of microstructured optical fiber," IEEE Photon. Technol. Lett. **18**, 511– 513 (2006).

#118110 - $15.00 USD Received 2 Oct 2009; revised 30 Oct 2009; accepted 30 Oct 2009; published 11 Nov 2009

11. T. Wei, Y. Han, H. L. Tsai, and H. Xiao, "Miniaturized fiber inline Fabry-Perot interferometer fabricated with a femtosecond laser," Opt. Lett. **33**, 536–538 (2008).
12. J. Villatoro, V. Finazzi, V. P. Minkovich, V. Pruneri, and G. Badenes, "Temperature-insensitive photonic crystal fiber interferometer for absolute strain sensing," Appl. Phys. Lett. **91**(9), 091109 (pages 3) (2007).
13. H. Y. Choi, K. S. Park, and B. H. Lee, "Photonic crystal fiber interferometer composed of a long period grating and one point collapsing of air holes," Opt. Lett. **33**(8), 812–814 (2008).
14. G. Coviello, V. Finazzi, J. Villatoro, and V. Pruneri, "Encapsulated and coated photonic crystal fibre sensor for temperature measurements up to 1000°C," in *CLEO EUROPE - EQEC 2009. Conference on lasers and electro-optics - European Quantum Electronics Conference*, p. CH1.6 (2009).
15. V. Finazzi, J. Villatoro, G. Coviello, and V. Pruneri, "Photonic Crystal Fibre Sensor for High Temperature Energy Environment," in *Optics and Photonics for Advanced Energy Technology*, p. ThC1 (Optical Society of America, 2009).
16. Y. Mohanna, J. Saugrain, J. Rousseau, and P. Ledoux, "Relaxation of internal stresses in optical fibers," J. Lightwave Technology, **8**(12), 1799–1802 (1990).
17. T. S. Izumitani, *Optical Glass* (American Institute of Physics, New York, USA, 1986).
18. J. E. Shelby, *Introduction to Glass Science and Technology*, 2^{nd} ed. (The Royal Society of Chemistry, Cambridge, UK, 2005).

1. Introduction

Fiber optic sensing has become one of the key applications of optical fibers in the last decades: exploiting the different ways in which the guiding mechanisms of an optical fiber can be modulated by external factors, such as pressure, liquid and gas presence, strain, temperature, has given rise to a large number of different approaches in the use of optical fibers in the field of sensing. Optical sensors have many advantages over their non-optical counterparts, amongst which being lightweight, accurate, compact and immune to electro-magnetic, radio-frequency, and microwave interference. Sensing in harsh environments, such as space vehicles, high power lasers, fire alarm systems, monitoring of furnace operation or volcanic events, requires reliable sensors with stability at ultra-high temperature.

Several issues arise when the temperature reaches very high values or when it gets close to the glass softening point. Doped fibers, for example, when subjected to very high temperatures for a long time suffer from dopant diffusion which modifies their guiding properties. Other effects are the so called fiber devitrification, i.e. the growth of a crystalline structure substituting the amorphous structure of the glass, and OH absorption [1, 2]. These effects can corrupt the guiding properties of the fiber and lead to a reduction of the mechanical strength, making unreliable the performance of high-temperature sensor based on doped fibers. To avoid these issues, sensors made from specialty optical fibers, such as fibers made from glasses with special composition, photonic crystal fibers (PCFs), or fibers with proper annealing treatment, have been proposed [3, 4, 5]. It is possible to categorize these high-temperature sensors in two classes. One involves the use of gratings while the other exploits interferometry [6, 7]. Most research groups focus on different types of gratings such as chemical composition gratings (CCG), long period gratings (LPGs), or regenerated fiber Bragg gratings (rFBGs) [8, 9, 4]. The fabrication of these gratings is complex since it involves tailoring the glass composition of the optical fiber, inscribing the gratings with femto-second lasers, or specific thermal or annealing processes. Interferometers, on the other hand, can be fabricated for example by tapering or combining different optical fibers [10, 11]. In spite of their simplicity interferometer-based high-temperature sensors can reach sensitivities comparable to that of gratings-based ones.

Here we report on a PCF-based two-mode interferometer suitable for ultra high temperature measurements. The device consists of a stub of index-guiding PCF fusion spliced between two single mode fibers (SMFs). In the splices the voids of the PCF are collapsed which allows the split and recombination of two core modes. To ensure stability of the device at high temperatures it was repeatedly annealed at 1000°C during several hours. This thermal treatment was found to be necessary to reach sensors with constant and repeatable functionality.

#118110 - $15.00 USD Received 2 Oct 2009; revised 30 Oct 2009; accepted 30 Oct 2009; published 11 Nov 2009

2. Device fabrication and theoretical analysis

To fabricate the modal interferometer here presented, a short piece of a home-made PCF, fabricated at Centro de Investigaciones en Óptica, Mexico, whose holes pattern is shown in figure 1a, was fusion spliced both sides to standard optical fiber (Corning SMF-28e) with an arc-discharge machine (Fitel S122A) using the conventional program to splice SMFs. Due to the heat necessary to fuse the two fibers, around the splicing zone, part of the holey structure of the PCF collapses (for a length of about 300 µm), as shown in figure 1f; in this collapsed region, the guiding structure of the PCF no longer exists and it is substituted by an all-silica rod. The first collapsed region is used to excite two modes into the PCF. Indeed, in the pure-silica region the fundamental SMF mode diffracts and, as a consequence, broadens allowing, due to the mismatch between this broadened Gaussian mode and the PCF, the excitation of two modes inside the PCF [12, 13, 14, 15]. Such modes propagate with different effective indices, and, consequently, with different phase velocities, through the uncollapsed region of PCF, until they recombine, through the second PCF collapsed zone, into the fundamental Gaussian mode of the second piece of SMF, creating an interferometric pattern. An example, characterized by an insertion loss of about 9 dB and a contrast of about 13dB, is shown in figure 1e.

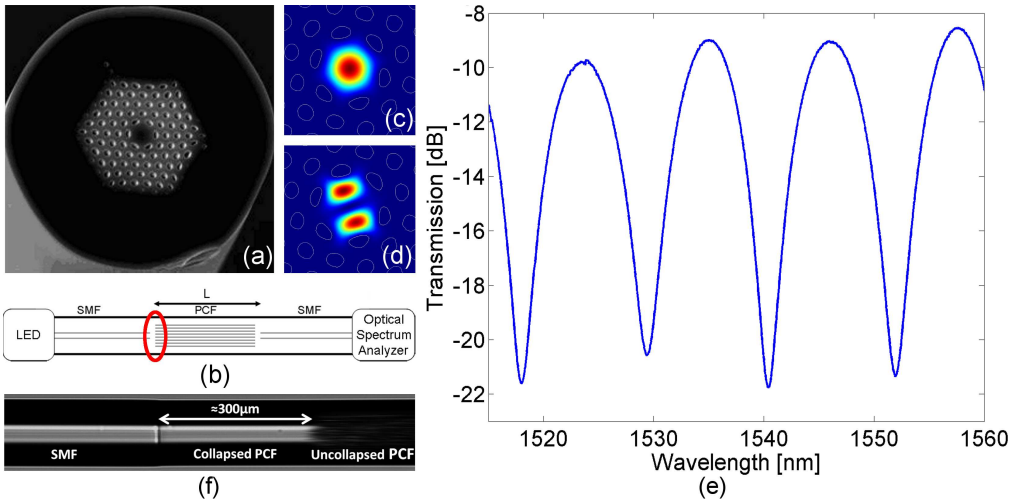

Fig. 1. (a) SEM image showing the hole pattern of the home-made fiber used to produce the devices. (b) Schematics of the proposed device, with the first splice zone, an image of which is shown in (f), highlighted. (c) The fundamental mode propagating into this kind of fiber, accordingly to our FEM simulations. (d) The second order mode propagating into our home-made PCF. (e) A typical interference pattern obtained with the discussed device: the length of this device was 22.6 mm, the period was about 11 nm, the insertion loss was 9 dB and the contrast about 13 dB. (f) Microscope image of the splice zone between the SMF, on the left, and the PCF, on the right. It is possible to see the 300 µm collapsed region and that the PCF holey structure far from the splice zone is not affected by the heat.

Assuming that only two modes exist in the uncollapsed section of the PCF, the intensity at the end of the PCF stub is

$$I = I_1 + I_2 + 2\sqrt{I_1 I_2}\cos\left(\frac{2\pi\Delta nL}{\lambda}\right) \tag{1}$$

where I_1 and I_2 are the intensities of the two interfering modes, L is the length of the device, and $\Delta n = n_1 - n_2$ is the difference between the effective indices of the two interfering modes.

#118110 - $15.00 USD Received 2 Oct 2009; revised 30 Oct 2009; accepted 30 Oct 2009; published 11 Nov 2009

The interferometric pattern changes as a function of the temperature because of two effects: the variation of n_1 and n_2 (and, consequently, of Δn) with temperature, due to thermo-optic effect, and the variation of the length of the device with temperature, due to thermal expansion:

$$\Delta n(T) \approx \Delta n(T_0) + \left.\frac{\partial \Delta n}{\partial T}\right|_{T=T_0} \Delta T \tag{2a}$$

$$L(T) \approx L(T_0)(1+\alpha_s \Delta T) \tag{2b}$$

where $\alpha_s = 5.5 \times 10^{-7}\ K^{-1}$ is the thermal expansion coefficient of silica. By subsituting equations 2a and 2b into 1, the thermal behavior of interference pattern is obtained:

$$I(T) \approx I_1 + I_2 + 2\sqrt{I_1 I_2}\cos\left(\frac{2\pi}{\lambda}\Delta n(T_0)L(T_0) + \frac{2\pi}{\lambda}\Delta n(T_0)\alpha_s L(T_0)\Delta T + \right.$$
$$\left. + \frac{2\pi}{\lambda}L(T_0)\left.\frac{\partial \Delta n}{\partial T}\right|_{T_0}\Delta T + \frac{2\pi}{\lambda}\alpha_s L(T_0)\left.\frac{\partial \Delta n}{\partial T}\right|_{T_0}\Delta T^2\right) \tag{3}$$

To the author's knowledge, up to now the temperature-induced variation of the effective index of a PCF high order mode (and, consequently, of Δn) has never been investigated, so, in order to predict the effective indices difference at room temperature and its variation with temperature, simulations were performed by means of Finite Element Method (FEM) using a commercial software package (COMSOL Multiphysics). The effective indices of the fundamental and higher order modes propagating into the fiber were calculated accounting for the difference in the refractive index of silica due to thermal effects, thus obtaining $\Delta n(T_0) \approx 6.5 \times 10^{-3}$ and $\partial \Delta n/\partial T|_{T=T_0} \approx -3 \times 10^{-8}\ \mathrm{K}^{-1}$. All the calculations were performed at the wavelength $\lambda_0 = 1550$ nm and the fiber geometry was obtained from SEM images of the PCF used during the experimental work (see figures 1a, 1b and 1c).

Using such values for $\Delta n(T_0)$, α_s and $\partial \Delta n/\partial T|_{T=T_0}$ and assuming that the temperature will assume the maximum value of $\approx 1000°$C, the second and fourth terms of the cosine phase in equation 3, i.e. the thermal expansion term and the second order term, respectively, are negligible, so that the equation simplifies in:

$$I(T) \approx I_1 + I_2 + 2\sqrt{I_1 I_2}\cos\left(\frac{2\pi}{\lambda}\Delta n(T_0)L(T_0) + \frac{2\pi}{\lambda}L(T_0)\left.\frac{\partial \Delta n}{\partial T}\right|_{T_0}\Delta T\right) \tag{4}$$

Furthermore, if the considered wavelength range ($\Delta\lambda$) is much smaller than the central wavelength ($\Delta\lambda \ll \lambda_0$), the following approximation is possible:

$$I \approx I_1 + I_2 + 2\sqrt{I_1 I_2}\cos\left(\frac{2\pi\lambda}{\Lambda} + \Delta\phi\right) \tag{5}$$

in which Λ is the period of the interferometric pattern and $\Delta\phi$ is its initial phase, respectively defined as:

$$\Lambda = \frac{\lambda_0^2}{\Delta n(T_0)L(T_0)} \tag{6a}$$

$$\Delta\phi = \frac{2\pi L(T_0)}{\lambda_0}\left.\frac{\partial \Delta n}{\partial T}\right|_{T=T_0}\Delta T \tag{6b}$$

The last equation establishes a direct relationship between the initial phase of the cosine and the temperature variation with respect to the initial temperature T_0. The variation of the initial

#118110 - $15.00 USD Received 2 Oct 2009; revised 30 Oct 2009; accepted 30 Oct 2009; published 11 Nov 2009

phase of this cosine implies a shift of the pattern with the temperature, which can be evaluated by writing the peak wavelength as a function of the initial phase:

$$\Delta\lambda_{peak} = -\frac{\Lambda}{2\pi}\Delta\phi = -\frac{\Lambda}{\lambda_0}\left.\frac{\partial\Delta n}{\partial T}\right|_{T=T_0} L(T_0)\Delta T \tag{7}$$

As $\partial\Delta n/\partial T|_{T=T_0}$ resulted to be negative in our simulations, a shift of the interferometric pattern towards higher wavelengths is expected when the temperature increases; furthermore the calculated device sensitivity is $\Delta\lambda/\Delta T \approx 7.15$ pm/K.

3. Experimental results and discussion

Several devices of different length were fabricated and characterized at room temperature to determine the effective indices difference between the two modes. Light from a broadband source, centered at $\lambda_0 = 1550$ nm and with a span $\Delta\lambda = 60$ nm, was launched to the devices and the output was fed to a computer controlled optical spectrum analyzer. In figure 2a the different occurrences of Δn are plotted. The average value is 9.54×10^{-3}, with a standard deviation of 1.29×10^{-3}, in good agreement with the results of the FEM simulations. In figure 2b the measured interferometric patterns periods are plotted as a function of the devices length, along with the theoretical prediction, obtained using the average value of Δn in equation 6a.

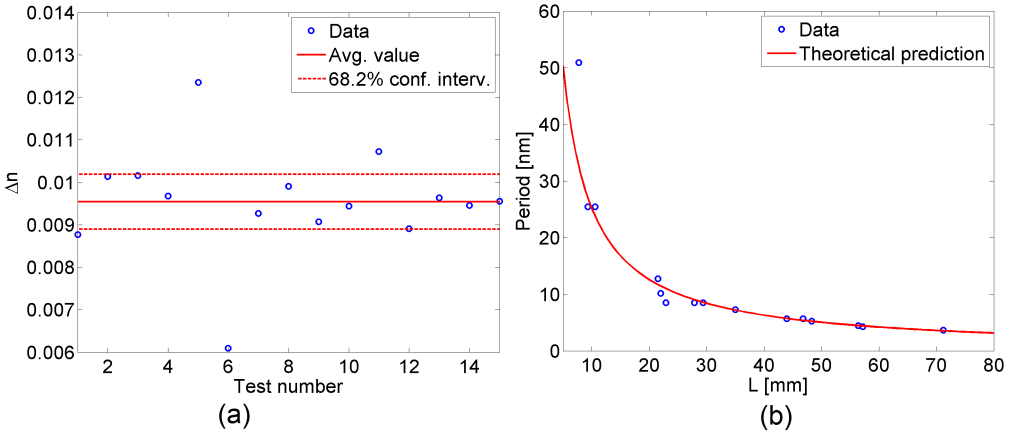

Fig. 2. (a) Measured values of the indices difference, their average value and the confidence interval. (b) Measured periods plotted as a function of the device lengths (circles) and the fit obtained using the average value of Δn of 9.54×10^{-3}.

In order to reduce the glass internal stresses and eventual core ellipticity, the fiber device was annealed. We performed the annealing on a device of PCF length at room temperature equal to $L(T_0) \approx 22.6$ mm, so that the obtained period was $\Lambda = 11.7$ nm. The device was enclosed in a tubular oven capable of reaching a temperature of 1200°C, at a maximum rate of ≈ 60°C/min. The temperature inside the oven was monitored through a thermocouple located close to the device, whose output was connected to an optical spectrum analyzer. A Fourier transform was performed on every acquired trace and the initial phase of the pattern's dominant component was subtracted to the initial phase of the same pattern component at room temperature, thus obtaining the phase difference from which the pattern shift was calculated by means of equation 7.

In figure 3, the temperature inside the oven and the shift of the pattern are plotted as functions of time. The temperature cycle consisted in an increment of the temperature inside the

#118110 - $15.00 USD Received 2 Oct 2009; revised 30 Oct 2009; accepted 30 Oct 2009; published 11 Nov 2009

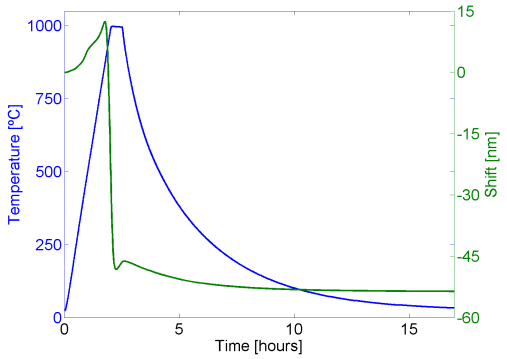

Fig. 3. Experimental result of the first temperature cycle. The blue curve shows the temperature inside the oven as measured by the thermocouple, while the green curve shows the pattern shift, with the drop starting at a temperature of $\approx 850^{\circ}$C.

oven chamber up to 1000°C at a rate of 10°C/min, the temperature was then kept constant for two hours and, finally, the oven was left to passively cool down. The device response resulted particularly interesting: after observing the expected shift of the pattern towards higher wavelengths, when the temperature reached $\approx 850^{\circ}$C, the pattern started shifting very fast towards lower wavelengths at a rate of about -470 pm/K, until the temperature reached the maximum; after this rapid shift, the pattern started again shifting towards higher wavelengths, although the temperature was constant. When the temperature started to decrease, the pattern accordingly moved towards lower wavelengths and, at the end of the process, when the temperature had been brought back to room temperature, the total difference between the pattern final and starting positions was equal to -53.56 nm.

We believe that the drop shown in figure 3 is probably due to relaxation of internal stresses frozen in the fiber during drawing [16] and that the shift of the pattern towards higher wavelengths, although kept at a fixed temperature, is due to the variation of the glass fictive temperature, which has an impact on the glass structure and, consequently, also on several glass properties, among which the refractive index [17, 18]; in order to further stabilize the device behavior at high temperatures, four more temperature cycles were performed, as shown in figure 4. In these cycles, the temperature was pushed up to 1000°C as fast as the oven allowed us, then it was kept constant for several hours, and finally the oven was left to passively cool down. In these tests, the device did not show the drop previously described, but the effect of the thermal annealing continued being observed: indeed, once the temperature of 1000°C had been reached, the interference pattern continued shifting although the temperature was kept constant, thus showing that the fictive temperature had not reached yet its final value. In the second test (figure 4a), two different shift rates could be observed: in the first 2.25 hours in which the temperature was 1000°C, the pattern shifted at a rate of 3.95 nm/hour, while during the last 4.13 hours, the shift rate was 1.40 nm/hour. After the device was cooled down, the difference between the final and initial positions of the pattern was equal to 15.83 nm. During the third and the fourth cycles (figures 4b and 4c, respectively), the pattern shift rate at 1000°C kept decreasing, being 0.50 nm/hour and 0.19 nm/hour, respectively. The differences between the positions of the interferometric pattern at the beginning and at the end of the thermal cycle decreased as well, being equal to 4.15 nm and 1.04 nm respectively. Finally, during the fifth thermal cycle (figure 4d), the shift rate and the difference between the initial and final positions of the pattern were practically negligible so we assumed that, after this cycle, the processes of

#118110 - $15.00 USD Received 2 Oct 2009; revised 30 Oct 2009; accepted 30 Oct 2009; published 11 Nov 2009

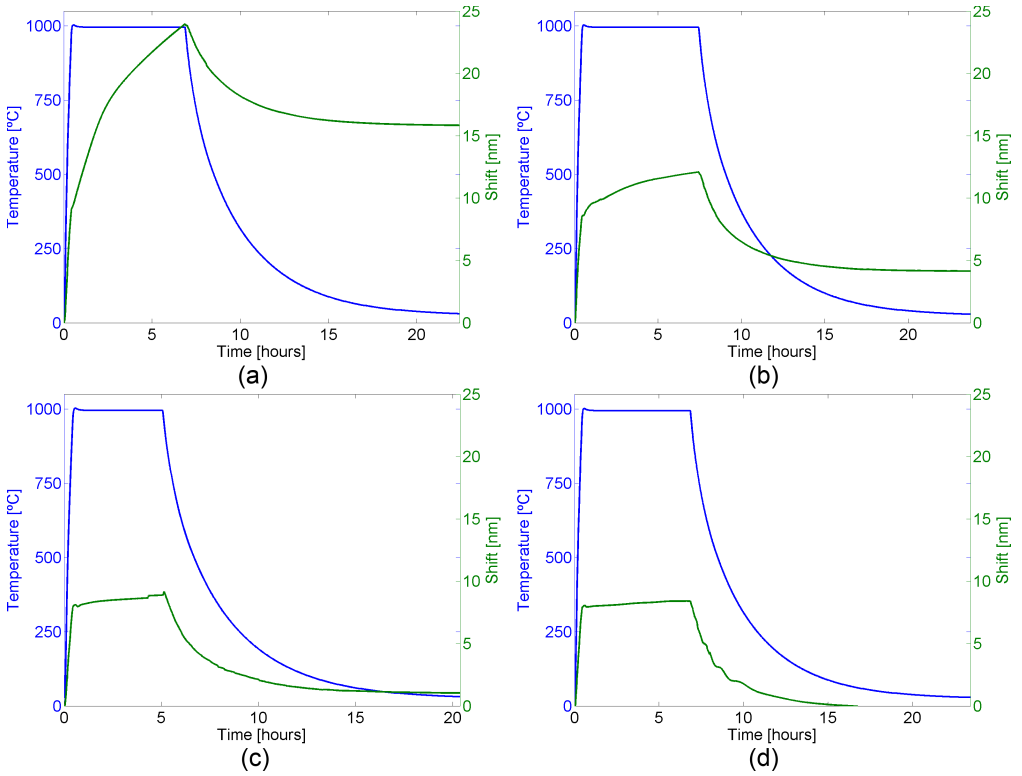

Fig. 4. The temperature cycles used to anneal the device. In all of them the temperature was pushed up to 1000°C as fast as possible, then it was kept constant for several hours, then the oven was passively cooled down.

relaxation of the fiber's internal stresses and of the glass structure were both concluded. Note that even though in this paper only results related to a single fiber device are presented, similar behaviors have been observed in other devices fabricated in the same way, although the drop rate, during the first cycle, and the shift rates, during the successive cycles, change if the fiber type or brand is changed: we reckon that this effect is due to different drawing conditions and to different starting fictive temperatures.

In figure 5a the differences between the final and initial positions of the pattern for each temperature cycles are plotted as a function of the cycle number: the convergence towards 0 of this difference can be appreciated as the burn-in (thermal annealing) process is being completed. Figure 5b shows the cumulative pattern shift versus temperature of all the subsequent temperature cycles: it can be noticed that for the last cycle (black curve), the curves relative to the heating-up and cooling-down phases perfectly overlap.

After the burn-in process, we fitted the curve of the wavelength shift versus temperature of device during the last thermal cycle using equation 7, leaving as free parameter the thermal dependence of the difference between the two refractive indices, i.e. $\partial\Delta n/\partial T|_{T=T_0}$. This results in $\partial\Delta n/\partial T|_{T=T_0} = -5.094\times10^{-8}\,K^{-1}$, which implies a sensitivity $\Delta\lambda/\Delta T = 8.3$ pm/K, slightly higher than the one calculated through the theoretical analysis.

To check the functionality of the device after the burn-in we performed a sixth experiment. During this test, the temperature was brought to 1000°C through some steps, at 200°C, 400°C, 600°C, 700°C, 800°C and 900°C, during which it was kept constant for half a hour; when the

#118110 - $15.00 USD Received 2 Oct 2009; revised 30 Oct 2009; accepted 30 Oct 2009; published 11 Nov 2009

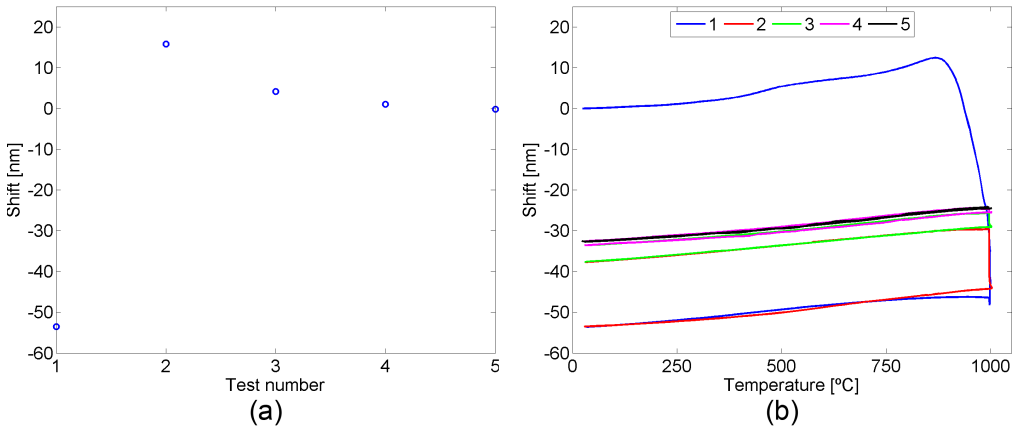

Fig. 5. (a) Plot of the differences between the starting and ending positions of the pattern during the different temperature tests. (b) Plot of the cumulative pattern shift during the first five temperature cycles.

temperature had reached 1000°C, it was kept constant for half a hour before cooling down the oven. The results of this test are shown in figure 6, and again we found that the difference between the initial and final position of the pattern were practically negligible.

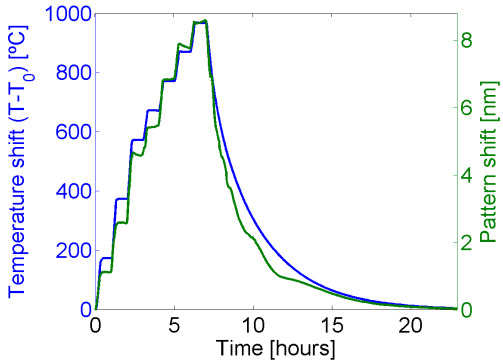

Fig. 6. Sixth temperature cycle. In blue it is plotted the temperature as measured by the thermocouple, in green the pattern shift.

4. Conclusions

The fabrication and thermal stabilization of a Photonic Crystal Fiber (PCF) based two-mode-interferometric sensor, designed for ultra-high temperature measurements ($\leq$1000°C), has been reported. The fabrication of the device is simple since it consists of a stub of PCF spliced to standard optical fibers. The first splicing region allows for the excitation of two core modes into the PCF, which form the interferometric pattern when recombining through the second splicing region. The device response is a sinusoidal pattern that, because of thermo-optic effect, shifts with temperature. We found that the sensor head needs to be treated with few thermal cycles in order to eliminate internal stresses *frozen* in the fiber structure during drawing, and that such a thermal treatment also results in a change of the fiber guiding properties related to changes

#118110 - $15.00 USD Received 2 Oct 2009; revised 30 Oct 2009; accepted 30 Oct 2009; published 11 Nov 2009

in glass the fictive temperature. The resulting device is stable and allows repeatable ultra-high temperature measurements with a sensitivity $\Delta\lambda/\Delta T \approx 8.3$ pm/K.

Acknowledgments

The authors are grateful to Dr. Vladimir P. Minkovich for providing PCFs and to Dr. Sarah Benchabane for helping in getting SEM pictures of PCFs. This work was carried out with the financial support of the European Space Agency through grant ITI 21798/08/NL/CBI and of Ministerio de Ciencia e Innovación / Ministerio de Fomento (Spain) through the project SOPROMAC No. P41/08. Vittoria Finazzi and Joel Villatoro acknowledge funding from the Ministerio de Educación y Ciencia (Spain) through the "Ramón y Cajal" program.

#118110 - $15.00 USD Received 2 Oct 2009; revised 30 Oct 2009; accepted 30 Oct 2009; published 11 Nov 2009